ORIGINAL RESEARCH

Anatomical characterization of the inferior petrosal sinus and adjacent cerebellopontine angle cistern for development of an endovascular transdural cerebrospinal fluid shunt

Carl B Heilman,[1,2] Gregory W Basil,[2] Brandon M Beneduce,[3] Adel M Malek[1,2]

[1]Department of Neurosurgery, Tufts Medical Center, Boston, Massachusetts, USA
[2]Tufts University School of Medicine, Boston, Massachusetts, USA
[3]CereVasc LLC, Auburndale, Massachusetts, USA

Correspondence to
Dr Adel M Malek, Cerebrovascular and Endovascular Division, Department of Neurosurgery, Tufts Medical Center, Boston MA 02111, USA; amalek@tuftsmedicalcenter.org

Received 20 September 2018
Revised 19 October 2018
Accepted 19 October 2018

Check for updates

© Author(s) (or their employer(s)) 2019. No commercial re-use. See rights and permissions. Published by BMJ.

To cite: Heilman CB, Basil GW, Beneduce BM, *et al*. *J NeuroIntervent Surg* Epub ahead of print: [*please include* Day Month Year]. doi:10.1136/neurintsurg-2018-014445

ABSTRACT

Background and purpose We evaluated the inferior petrosal sinus (IPS) and adjacent cerebellopontine angle (CPA) cistern as a potential implantation site for a novel venous endovascular transdural CSF shunt concept to treat communicating hydrocephalus. We analyzed the dimensions of the IPS, CPA cistern, and distances to adjacent neurovascular structures.

Materials and methods Gadolinium enhanced T1 weighted brain MRI datasets of 36 randomly selected patients, aged 20–80 years, were analyzed with three-dimensional multiplanar reconstruction to measure IPS diameter and length, CPA cistern depth, and IPS proximity to the vertebrobasilar arteries and brainstem. Statistical analysis was used to assess gender, sidedness, and age dependence.

Results Mean IPS diameter ranged from 2.27 mm to 3.31 mm at three axial levels, with >90% larger than 1.46 mm. CPA cistern adjacent to the IPS exhibited a mean depth of 3.86 mm to 7.39 mm between the dura and brainstem at corresponding axial levels. There was no side dependence except for a longer distance from the IPS to the basilar artery on the left compared with the right (9.72 vs 7.28, P<0.019). Linear regression analysis showed that the distance from the IPS to the brainstem was statistically significantly increased with age (P<0.0002) and was greater in men, with little side variation (P=0.524).

Conclusion Our results demonstrate sufficient CSF CPA cisternal space adjacent to the IPS and support the feasibility of an endovascular catheter delivered transdural implantable shunt. Such a device could serve to mimic the function of the arachnoid granulation by establishing a regulated path for CSF flow from the intracranial subarachnoid space to the venous system and provide a treatment for communicating hydrocephalus.

INTRODUCTION

Communicating hydrocephalus is characterized by an abnormal accumulation of CSF within the intracranial cavity in the absence of a physical obstruction between the lateral ventricles and the subarachnoid space. Conventional surgical treatment involves the implantation of a ventriculoperitoneal shunt to divert excess CSF[1] although ventriculoatrial and ventriculopleural shunts are also employed on occasion as well as endoscopic third ventriculostomy.[2] Numerous technological advancements for the CSF shunt valve design have been made in an effort to improve device function and alleviate associated complications. However, complications remain frequent and contribute to shunt failure rates as high as 40% in the first 2 years following implantation.[3–5] New technologies that reduce or eliminate complications associated with current CSF shunts are needed.

A possible novel approach aims to mimic arachnoid granulation function by diverting excess CSF from the intracranial subarachnoid space to the adjacent cerebral venous system through an endovascular transdural shunt device. Such an endovascular shunt, which could be delivered through a transvenous transfemoral approach to puncture and bridge the dura, would rely on the positive pressure gradient between intracranial and venous pressures to regulate CSF flow.[6]

A potential target location for neurointerventional transdural venous delivery for an endovascular shunt was identified as the inferior petrosal sinus (IPS) (figure 1A), the dural venous sinus that travels along the skull base at the posterior–inferior edge of the petrous bone, lateral to the clivus, and drains blood from the cavernous sinus into the internal jugular vein.[7] The position of the IPS adjacent to the large CSF filled cerebellopontine angle (CPA) cistern, provides a potential site for an endovascular shunt to transdurally shunt CSF to the venous system.

The anatomy of the IPS is familiar to the neuroendovascular operator given its importance in procedures such as IPS venous sampling for Cushing's syndrome and transvenous treatment of carotid–cavernous fistulas.[7–9] Furthermore, recent publications have characterized the various patterns of the IPS confluence with the internal jugular vein, providing critical information for IPS catheterization.[10–12] Nonetheless, detailed measurements of IPS caliber and adjacent CPA cistern depth are not available.

To assess the viability of the IPS as a target deployment site for an endovascular CSF shunt, we set out to measure IPS diameter and length, CPA cistern depth, and IPS proximity to critical neurovascular structures. In this study, we analyze these measurements and their dependence on age, gender, and side, and provide a predictive model for the target CSF space for a potential endovascular CSF shunt.

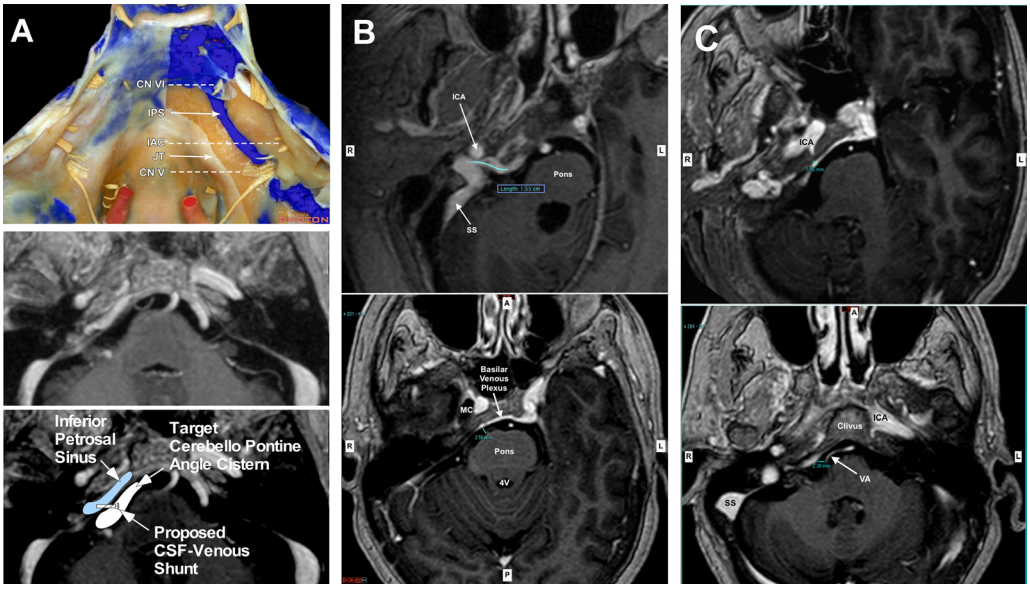


Figure 1 (A) Cadaver dissection of the region of interest from *The Rhoton Collection* under license: https://creativecommons.org/licenses/by-nc-sa/4.0/legalcode(top). Gadolinium enhanced T1 weighted MRI of the region of interest (center) delineating the inferior petrosal sinus (IPS, bottom, light blue), target cerebellopontine angle cistern (white), and a schematic of the proposed deployment site of the endovascular transdural CSF shunt (bottom). (B) Illustration of measurements for 'length of IPS from the jugular bulb to the jugular tubercle' (top) and 'distance from the brainstem to the IPS at CN VI' (bottom). (C) Sample measurements for 'diameter of the IPS at the IAC' (top) and 'shortest distance from the IPS to the VA' (bottom). 4V, fourth ventricle; CN, cranial nerve; IAC, internal auditory canal; ICA, Internal carotid artery; JT, jugular tubercle; MC, Meckel's cave; SS, sigmoid sinus; VA, vertebral artery.

MATERIALS AND METHODS

Study population

This study was approved by the institutional review board of Tufts Medical Center (IRB No 11639). Six cohorts each consisting of three men and three women from the institution's gamma knife imaging database, having all undergone a sub 1 mm T1 weighted post-gadolinium brain MRI, were selected at random from the following six age ranges for a total of 36 patients: 20–30, 30–40, 40–50, 50–60, 60–70, and 70–80 years of age at the time of imaging. Patients with pathologic conditions involving the skull base, brainstem, or posterior fossa in the region of the IPS or CPA cistern were excluded.

Measurements and MRI analysis

Measurements were made in three-dimensional multiplanar reconstruction mode with OsiriX MD imaging software (Pixmeo, Geneva, Switzerland); IPS diameter was measured orthogonal to its multiplanar course at three axial levels as the IPS traverses from the jugular bulb to the cavernous sinus at the (a) jugular tubercle, (b) internal auditory canal (IAC), and (c) entrance of cranial nerve VI (CN VI) into Dorello's canal (figure 1B,C). IPS length was measured along its course, with three-dimensional multiplanar reconstruction identifying optimal viewing plane, from its jugular bulb confluence to the IPS location corresponding to the same three axial levels ((a)–(c) above).

CPA cistern depth was measured as the orthogonal distance between the brainstem edge to the IPS bordering the CPA cistern, at the three axial levels ((a)–(c)). In addition, we measured the shortest lateral (left to right) distance between the IPS and the (1) vertebral arteries (VA) and (2) basilar artery (BA). These measurements were recorded in the axial imaging plane and identified by evaluating each MRI slice that showed the IPS, between the levels of the jugular tubercle and CN VI, bilaterally, except in certain cases where the VA or BA was not clearly identifiable on axial MRI slices between the jugular tubercle and CN VI. Figure 1B,C provide example measurement recordings to further demonstrate the methods. Figure 1A provides a sample image adapted from *The Rhoton Collection*[13] that depicts the IPS along the skull base with corresponding axial levels evaluated in this study.

Statistical analysis

Paired t test, linear regression, matched pair analysis, and univariate and multivariate analysis of variance were used to analyze the measurements and evaluate dependence on age, gender, and sidedness using JMP V.13 (SAS Institute Inc, Cary, North Carolina, USA). A P value of <0.05 was assumed for statistical significance.

Table 1 Mean, median, and 10th percentile values for each measurement across the entire study population

Measurement	N	Mean±SD (mm)	Median (mm)	10th percentile (mm)
Diameter of IPS at JT	72	3.31±0.98	3.42	1.82
Diameter of IPS at IAC	72	2.81±0.96	2.62	1.62
Diameter of IPS at CN VI	72	2.27±0.64	2.22	1.46
Length of IPS from JB to JT	72	13.8±1.95	14.2	11.0
Length of IPS from JB to IAC	72	19.4±2.79	19.33	16.6
Length of IPS from JB to CN VI	72	31.4±4.51	31.3	25.8
Distance from IPS to BS at JT	72	7.39±2.52	7.26	4.43
Distance from IPS to BS at IAC	72	4.38±1.89	4.31	1.76
Distance from IPS to BS at CN VI	72	3.86±1.68	3.53	1.64
Shortest distance from IPS to VA	50	3.52±2.92	2.72	0.9
Shortest distance from IPS to BA	70	8.75±3.49	8.54	4.2

BA, basilar artery; BS, brainstem; CN, cranial nerve; IAC, internal auditory canal; IPS, inferior petrosal sinus; JB, jugular bulb; JT, jugular tubercle; VA, vertebral artery.

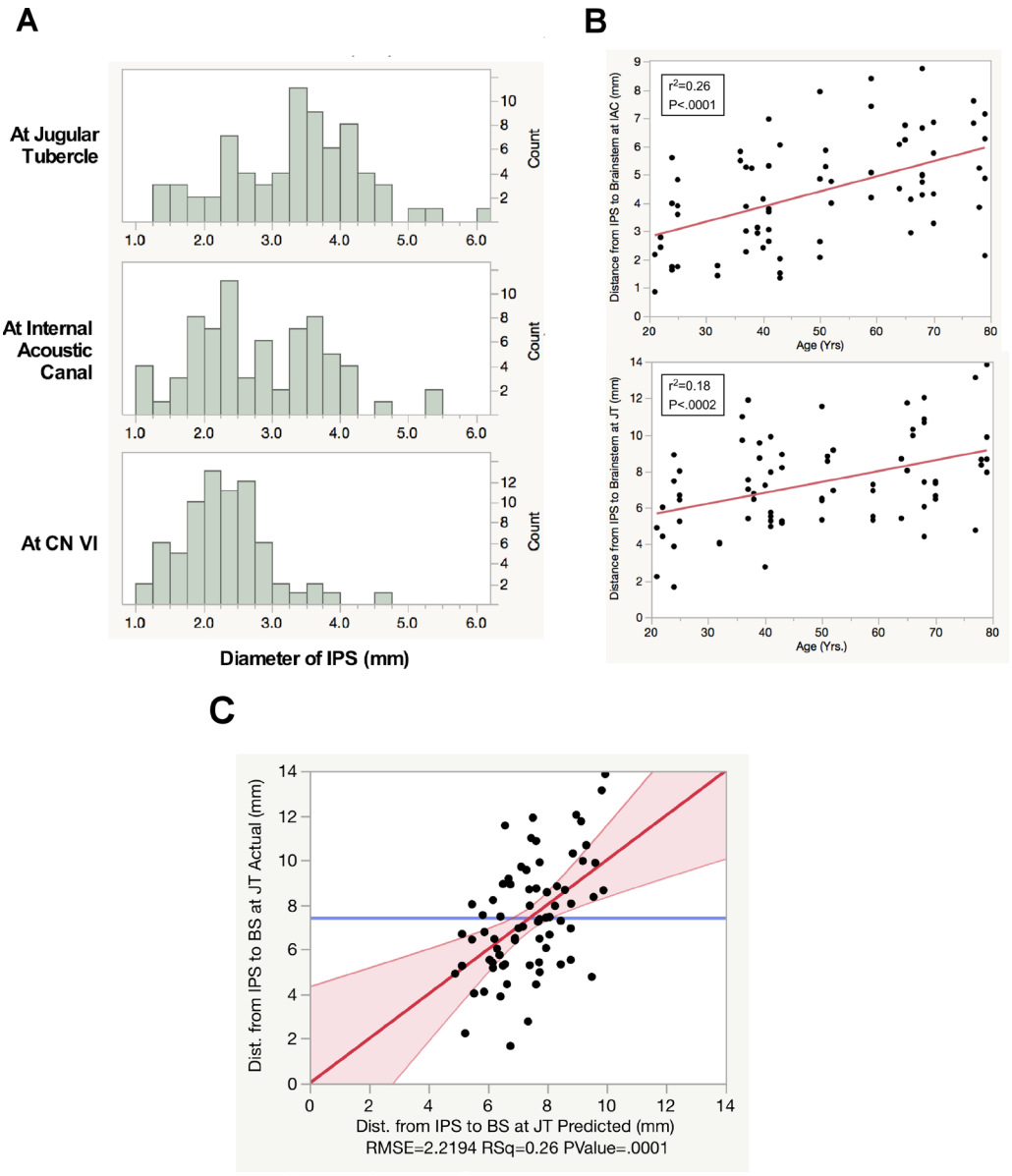


Figure 2 (A) Histogram of measured inferior petrosal sinus (IPS) diameter at the jugular tubercle (top), internal acoustic canal (middle), and at the level of the cranial nerve (CN) VI (bottom). (B) Distance from the IPS to the brainstem (BS) at the level of the internal acoustic canal (IAC, top) and jugular tubercle (JT, bottom) with respect to patient age, showing a linear correlation. (C) Multivariate model showing predicted versus actual distance from the IPS to the BS at the level of the JT; significance of age and gender but not sidedness (with 95% CI).

RESULTS

Table 1 provides the total number of measurements with corresponding means (SD), medians, and values at the 10th percentile. Mean IPS diameter was largest at the level of the jugular tubercle (3.31 mm) and became progressively smaller as the vessel approached the cavernous sinus at the level of the IAC (2.81 mm) and CN VI (2.27 mm). Note that the IPS diameter was larger than 1.46 mm at any level in >90% of measured IPS (figure 2A). Adjacent to the IPS, the CPA cistern exhibited the largest mean depth at the level of the jugular tubercle (7.39 mm) and decreased in depth as it progressed rostrally at the levels of the IAC (4.38 mm) and CN VI (3.86 mm).

Age dependence of the measured anatomical parameters was assessed using linear regression and this revealed a significant age dependent increase in the distances from the IPS to the brainstem at all levels ($P<0.0002$ in all cases) (figure 2B). There was no discernible age dependence on any of the other measurements of the IPS, or distances (table 1).

Matched pair analysis using sidedness revealed no differences in distance from the IPS to the brainstem at the jugular tubercle, or at the IAC, but showed a greater distance from the IPS to the brainstem on the left compared with the right (4.12 vs 3.61 mm, $P<0.01$) (table 2). Similar matched pair analysis revealed no statistically significant sidedness dependence on distance from the IPS to the VA, but greater distance from the left IPS to the BA compared with the right (9.72 vs 7.79 mm, $P<0.021$). There was no matched side difference in IPS diameter or IPS length at any of the three measurement levels.

In order to determine the relative contribution of age, gender, and side, a general linear model was used with age as the continuous and gender/side as the categorical variable to analyze the important variables that may be critical for consideration in

Table 2 Univariate analysis of measured parameters versus the side of the inferior petrosal sinus and patient gender

Left to right side difference	Right	Left	P values
Distance from IPS to BS at CN VI (mm)	3.61±1.59	4.11±1.74	0.204
Shortest distance from IPS to BA (mm)	7.78±4.11	9.72±2.41	**0.019**
Gender differences	**Men**	**Women**	**P values**
Distance from IPS to BS at JT (mm)	8.12±2.88	6.67±1.88	**0.014**
Distance from IPS to BS at IAC (mm)	4.87±1.76	3.89±1.92	**0.028**
Distance from IPS to BS at CN VI (mm)	4.29±1.77	3.43±1.49	**0.029**
Length of IPS from JB to IAC (mm)	20.05±2.80	18.7±2.64	**0.038**

Values are mean (±SD).
BA, basilar artery; BS, brainstem; CN, cranial nerve; IAC, internal auditory canal; IPS, inferior petrosal sinus; JB, jugular bulb; JT, jugular tubercle.

targeting the transdural puncture for the proposed endovascular CSF shunt, at the level of the jugular tubercle (figure 2C).

This led to a model showing high significance for age ($P<0.0002$) and gender ($P<0.0119$) but not sidedness ($P<0.5241$) with a prediction formula for estimation of the distance from the IPS to the brainstem (BS) at the jugular tubercle as follows (in mm) (Table 3):

$D_{IPS\text{-}BS}=4.52+[-0.676(\text{if gender=female}) \text{ or } +0.676(\text{if gender=male})]+(0.058*\text{Age})+[-0.168(\text{if side=right}) \text{ or } +0.168(\text{if side=left})]$

DISCUSSION

The current study set out to evaluate the anatomical age and gender dependence of the IPS and adjacent CPA cistern and its neurovascular structures to evaluate the feasibility and derive relevant design parameters for an endovascular CSF shunt device that would be transvenously deployed in the IPS where it would breach the dura and establish a cisternal venous CSF pathway.

IPS diameter

Based on the current results, a 4 F (1.33 mm) endovascular catheter could be readily maneuvered and deployed into the IPS for a large proportion of patients. Specifically, the data showed IPS average diameter to be >1.33 mm at all three axial levels, with all study patients having at least one IPS (right or left) diameter >1.33 mm at all three axial levels. It should be noted that in some patients the IPS exists as multiple channels or a plexus near its confluence with the jugular bulb.[10–12 14] Small focal webs or duplicate channel openings may be too small to identify on MRI. In addition, the narrowest portion of the IPS can occasionally exist just as the IPS passes the lower cranial nerves at the medial aspect of the jugular bulb. To our knowledge, this is the first report to describe a comprehensive analysis of IPS sizing and a detailed statistical analysis of age, sex, and laterality differences.

Published literature describing the IPS has primarily focused on venous drainage pattern types and prevalence rates for IPS confluence with the internal jugular vein bulb.[10–12 14] This has provided ample information for neurointerventionalists aiming to catheterize the IPS for procedures such as bilateral IPS sampling and embolization of carotid–cavernous fistulas. Despite the variety of observed confluence patterns, it is generally accepted that the IPS junction with the jugular vein can be routinely accessed using a 5 F catheter.[7 10]

Some research groups have attempted to measure IPS diameter non-invasively. Tanoue *et al*[15] used multidetector row CT to identify the largest diameter of the minimum axis of the IPS on transverse images, at a mean of 0.99 mm and 2.04 mm on the right and left sides, respectively. Zhang *et al*[12] utilized multislice spiral CT and measured IPS diameter at the cranial exit to be similar bilaterally at 1.95 mm (right) and 1.96 mm (left), and at the internal jugular confluence to be significantly larger on the right (2.65 mm vs 2.36 mm). Bošković *et al*[16] using an anatomic study of human skulls described an IPS diameter of 7–10 mm at the cavernous sinus and 2–4 mm at the jugular foramen. Our study identified IPS mean diameter at three axial levels (mean 2.27–3.31 mm) comparable with the previous literature, with the exception of the cavernous sinus values of Bošković *et al*.[16]

IPS length

IPS length provides important design information for the venous portion of the proposed endovascular shunt and in determining where the CSF outlet will rest following deployment. Over-drainage, a frequent complication of conventional CSF shunts, arises due to the large posture dependent hydrostatic pressure column that can be created with long distal catheters.[17] The proximity of the IPS to the CPA cistern allows for an implant to have a short length. Such a short endovascular CSF shunt, terminating within the IPS or internal jugular vein, could reduce the gravity dependent fluid column and resulting pressure gradient and decrease the extent of the over-drainage resulting from the siphon phenomenon . Bošković *et al*[16] reported that the IPS extends approximately 23–28 mm from the cavernous sinus to the internal jugular vein, similar to our recorded mean IPS length of 31.4 mm from the jugular bulb to the axial level of CN VI[16]. Other published literature describes only the extracranial length of the IPS when its confluence with the internal jugular vein occurred below the jugular foramen.[12 18]

CPA cistern depth

To access CSF, a portion of an endovascular CSF shunt will need to reside within the confines of the CPA cistern. This study identified that the CPA cistern exhibits the largest depth adjacent to the IPS at the level of the jugular tubercle, with a mean of 7.39 mm. The CPA cistern then decreases in size rostral to this location (4.38 mm at the IAC and 3.86 mm at CN VI). Thus it is likely that the CPA cistern at the level of the jugular tubercle represents the largest pocket of CSF accessible via a neurointerventional approach and an ideal deployment location for an endovascular CSF shunt. In addition, our statistical analysis indicates that CPA cistern depth at the levels of the jugular tubercle

Table 3 Multivariate parameter estimate for distance from IPS to BS at JT with respect to gender, age and sidedness

Term	Estimate	Std Error	t Ratio	Prob>|t|	Lower 95%	Upper 95%
Intercept	4.523939	0.768176	**5.89**	**<0.0001***	2.9910674	6.0568106
Gender (F)	–0.676393	0.261845	**–2.58**	**0.0119***	–1.198895	–0.15389
Age	0.0579956	0.014591	**3.97**	**0.0002***	0.0288789	0.0871123
Side (left)	0.1675	0.261562	0.64	0.5241	–0.354439	0.6894389

and IAC may become greater with age and with male gender. We believe this is likely due to natural gray and white matter tissue atrophy that occurs during the normal aging process.[19]

To our knowledge, no comprehensive assessment of CPA cistern depth, between the IPS and brainstem, has been conducted. Some studies that have evaluated the pathogenesis of trigeminal neuralgia have described the trigeminal nerve cisternal length from Meckel's cave to the trigeminal nerve root entry zone.[20 21] Park *et al*[20] described the mean length of the trigeminal nerve cisternal segment on the unaffected side as 9.60 mm. Similarly, Parise *et al*[21] found a mean length on the unaffected side of 7.47 mm. While these studies provide measurements that approximate to the CPA cistern depth measured here, the location of the trigeminal nerve at the superior aspect of the CPA cistern is more rostral than the uppermost axial plane of measurement in our study, at the level of CN VI.

Although CPA cistern depth provides insight for identifying an implantation location that is a safe distance away from the brainstem, critical arterial structures residing within the CPA cistern must also be avoided. These vessels can readily be identified with preoperative imaging to select candidate patients and deployment locations. We found that the shortest distance from the IPS to the BA was significantly greater on the left (9.72 mm vs. 7.79 mm). It has been previously described that VA dominance may influence BA curvature through an opposite directional relationship.[22] As the left VA is typically the dominant vessel, it may cause the BA to more frequently reside on the right side of the CPA cistern, consistent with our findings.

Study limitations

Use of MRI to evaluate the size of the IPS, although not unprecedented,[23] is a limitation of this study, as it may not identify venous signal reliably and is dependent on imaging parameters.[24] Most literature evaluating IPS drainage patterns has relied on venographic approaches or higher resolution venous CT imaging.[10–12 14 15] Given the ability to microcatheterize angiographically occult or thrombosed inferior petrosal sinus in cases of carotid cavernous fistula,[8] it is likely that cross sectional non-invasive imaging may underestimate IPS diameter and also miss venous webs and strictures.

CONCLUSION

The current morphometric analysis demonstrates that the IPS and adjacent CPA cistern represent a possible deployment location for a transvenously delivered transdural endovascular CSF shunt, and can form the basis for design and development of such a device. Although the eventual preoperative planning will be patient based, the prediction formula derived from our measurements may assist operators in selecting candidates for safe endovascular deployment of the proposed CSF shunt.

Acknowledgements CereVasc LLC provided research stipend support to GWB for this study.

Contributors The image was obtained from the Rhoton collection and appropriately referenced as recommended by the source.

Funding CereVasc LLC provided research stipend support to GWB for this study.

Competing interests AMM and CBH are co-founders and investors of CereVasc, LLC. AMM, CBH, and BMB are shareholders of CereVasc, LLC.

Patient consent Not required.

Ethics approval The study was approved by Tufts Health Sciences Campus institutional review board.

Provenance and peer review Not commissioned; externally peer reviewed.

REFERENCES

1 Reddy GK, Bollam P, Caldito G. Ventriculoperitoneal shunt surgery and the risk of shunt infection in patients with hydrocephalus: long-term single institution experience. *World Neurosurg* 2012;78:155–63.
2 Madsen PJ, Mallela AN, Hudgins ED, *et al*. The effect and evolution of patient selection on outcomes in endoscopic third ventriculostomy for hydrocephalus: a large-scale review of the literature. *J Neurol Sci* 2018;385:185–91.
3 Al-Tamimi YZ, Sinha P, Chumas PD, *et al*. Ventriculoperitoneal shunt 30-day failure rate: a retrospective international cohort study. *Neurosurgery* 2014;74:29–34.
4 McAllister JP, Williams MA, Walker ML, *et al*. An update on research priorities in hydrocephalus: overview of the third National Institutes of Health-sponsored symposium "Opportunities for Hydrocephalus Research: Pathways to Better Outcomes". *J Neurosurg* 2015;123:1427–38.
5 Kofoed Månsson P, Johansson S, Ziebell M, *et al*. Forty years of shunt surgery at Rigshospitalet, Denmark: a retrospective study comparing past and present rates and causes of revision and infection. *BMJ Open* 2017;7:e013389.
6 Pollay M. The function and structure of the cerebrospinal fluid outflow system. *Cerebrospinal Fluid Res* 2010;7:9.
7 Miller DL, Doppman JL. Petrosal sinus sampling: technique and rationale. *Radiology* 1991;178:37–47.
8 Halbach VV, Higashida RT, Hieshima GB, *et al*. Transvenous embolization of direct carotid cavernous fistulas. *AJNR Am J Neuroradiol* 1988;9:741–7.
9 Yoshida K, Melake M, Oishi H, *et al*. Transvenous embolization of dural carotid cavernous fistulas: a series of 44 consecutive patients. *AJNR Am J Neuroradiol* 2010;31:651–5.
10 Miller DL, Doppman JL, Chang R. Anatomy of the junction of the inferior petrosal sinus and the internal jugular vein. *AJNR Am J Neuroradiol* 1993;14:1075–83.
11 Mitsuhashi Y, Nishio A, Kawahara S, *et al*. Morphologic evaluation of the caudal end of the inferior petrosal sinus using 3D rotational venography. *AJNR Am J Neuroradiol* 2007;28:1179–84.
12 Zhang W, Ye Y, Chen J, *et al*. Study on inferior petrosal sinus and its confluence pattern with relevant veins by MSCT. *Surg Radiol Anat* 2010;32:563–72.
13 Sorenson J, Khan N, Couldwell W, *et al*. The Rhoton Collection. *World Neurosurg* 2016;92:649–52.
14 Shiu PC, Hanafee WN, Wilson GH, *et al*. Cavernous sinus venography. *Am J Roentgenol Radium Ther Nucl Med* 1968;104:57–62.
15 Tanoue S, Kiyosue H, Sagara Y, *et al*. Venous structures at the craniocervical junction: anatomical variations evaluated by multidetector row CT. *Br J Radiol* 2010;83:831–40.
16 Bošković MSV, Josifov J. Über die Sinus petrosi und ihre Zuflüsse. *Gebenbaurs Morphol Jahrb* 1963;104:420–9.
17 Czosnyka Z, Czosnyka M, Richards HK, *et al*. Posture-related overdrainage: comparison of the performance of 10 hydrocephalus shunts in vitro. *Neurosurgery* 1998;42:327–34. discussion 33-4.
18 Gailloud P, Fasel JH, Muster M, *et al*. Termination of the inferior petrosal sinus: an anatomical variant. *Clin Anat* 1997;10:92–6.
19 Ge Y, Grossman RI, Babb JS, *et al*. Age-related total gray matter and white matter changes in normal adult brain. Part II: quantitative magnetization transfer ratio histogram analysis. *AJNR Am J Neuroradiol* 2002;23:1334–41.
20 Park SH, Hwang SK, Lee SH, *et al*. Nerve atrophy and a small cerebellopontine angle cistern in patients with trigeminal neuralgia. *J Neurosurg* 2009;110:633–7.
21 Parise M, Acioly MA, Ribeiro CT, *et al*. The role of the cerebellopontine angle cistern area and trigeminal nerve length in the pathogenesis of trigeminal neuralgia: a prospective case-control study. *Acta Neurochir* 2013;155:863–8.
22 Hong JM, Chung CS, Bang OY, *et al*. Vertebral artery dominance contributes to basilar artery curvature and peri-vertebrobasilar junctional infarcts. *J Neurol Neurosurg Psychiatry* 2009;80:1087–92.
23 Takahashi S, Sakuma I, Omachi K, *et al*. Craniocervical junction venous anatomy around the suboccipital cavernous sinus: evaluation by MR imaging. *Eur Radiol* 2005;15:1694–700.
24 Ouanounou S, Tomsick TA, Heitsman C, *et al*. Cavernous sinus and inferior petrosal sinus flow signal on three-dimensional time-of-flight MR angiography. *AJNR Am J Neuroradiol* 1999;20:1476–81.